

# GRAIN-SIZE EFFECT ON FATIGUE CRACK INITIATION CONDITION OBSERVED BY USING ATOMIC-FORCE MICROSCOPY

Y. Nakai, T. Kusukawa, and Y. Maeda

Department of Mechanical Engineering, Kobe University,  
1-1, Rokkodai, Nada, Kobe 657-8501, Japan

## ABSTRACT

Slip-band formation and fatigue crack-initiation processes in  $\alpha$ -brass were observed by means of atomic force microscopy (AFM), and the effects of the grain size, the stress amplitude, and the mean stress were discussed. In a fine grain material, fatigue cracks were initiated only from the slip-bands. In a coarse grain material, however, they were initiated either from the slip-bands or the grain boundaries. The depth of an intrusion drastically increased with its outgrowth to a crack, and with coalescence of cracks, the width of cracks increased rapidly. The depth of an intrusion increased with the number of loading cycles, and when the depth reaches a critical value, a transgranular crack was initiated from the intrusion. The critical value was given as a function of the slip-band angle relative to the stress axis. From the AFM observations, it was found that the critical value of the slip distance was independent of the slip-band angle relative to the stress axis, the stress amplitude, the mean stress, and the grain-size.

## KEYWORDS

Fatigue, Micromechanics, Crack-initiation, Slip-band,  $\alpha$ -brass, AFM

## INTRODUCTION

It is well known that the fatigue process of metallic materials without macroscopic defects can be divided into initiation and growth processes of cracks and final unstable fracture. Among these processes, various studies have been conducted on the crack-growth behavior, and that can be quantitatively analyzed based on the fracture mechanics [1]. The initiation condition of fatigue micro-cracks, however, still has not clarified enough, because no method for successive, direct and quantitative observation of the process had been devised. The study on the fatigue crack initiation is especially important for the fatigue damage evaluation of micro-machine components because most of the fatigue life of these components is occupied by the crack initiation life [2].

For components without significant internal defects, free surface is normally the site for fatigue crack initiation, then microscopic observation is the most useful method to clarify the mechanisms of fatigue processes in materials, and the progress of metal fatigue study has strongly depended on the development of new microscopic

observation methods.

With conventional microscopes, such as optical microscopes (OM), transmission electron microscopes (TEM), and scanning electron microscopes (SEM), however, successive, quantitative three-dimensional observations of the crack nucleation portion in the specimen surface could not be conducted. In most of these studies, the crack-initiation mechanisms were discussed qualitatively. Since the surface morphology of materials can be observed with atomic-scale resolution, the scanning atomic force microscopy (AFM) is a powerful technique to study mechanisms of fatigue and fracture of solid materials. Nakai and his co-workers studied fatigue slip-bands, fatigue crack-initiation, and the growth behavior of micro-cracks in a structural steel [3], and  $\alpha$ -brass [4, 5, 6].

In our previous study for  $\alpha$ -brass, slip-band formation and fatigue crack-initiation processes were observed by means of AFM [4, 5]. Surface of a fatigued specimen was observed at the maximum stress, unloading state, and the minimum stress at the same number of cycles. In the initial stage of the fatigue process, slip-bands, which were formed only under tension stress or compression stress, were observed. These kinds of slip-bands, however, disappeared shortly. Under tension stress, cracks could be detected easily with the AFM image just after their initiation. Before crack-initiation, the height and the width of extrusions and the depth and the width of intrusions gradually increased with the number of cycles. When slip-bands developed cracks, one of these sizes was changed drastically, where sizes to be changed depended on the slip-band angle relative to the stress-axis and the shape of slip-bands. The shape of slip-bands tips was also observed, and they were compared with the results from the continuum distributed dislocation theory. The slip-bands had steep slope when they were blocked by grain boundaries, and the slip-bands descended by gradual slopes to plain surfaces when they terminated within grains [6].

In the present paper, slip-band formation and fatigue crack-initiation processes in  $\alpha$ -brass were observed by means of AFM, and the conditions for the crack-initiation was discussed.

## EXPERIMENTAL PROCEDURE

The material for the present study was 70-30 brass ( $\alpha$ -brass). The chemical composition of the material (in mass %) was as follows: 69.92 Cu, 30.07 Zn, 0.0071 Fe, and 0.0026 Pb. After the specimens were made by the electric-discharge machining, they were heat treated at 320 °C for 180 s (Material A), or at 850 °C for 3600 s (Material B). The grain sizes of Material A and B were 20  $\mu\text{m}$  and 1,100  $\mu\text{m}$ , respectively. Before fatigue tests, surface of the specimens were electro-chemically polished. The specimen has a minimum cross-section of width 8 mm, and a thickness of 3 mm. It has a weak stress concentration with the elastic stress concentration factor of 1.03 under plane bending [4]. Since most of fatigue cracks were not initiated from the shallow notch root, the stress concentration factor was not considered in the calculation of the stress amplitude. The fatigue tests were carried out in a computer-controlled electro-dynamic vibrator operated at a frequency of 30 Hz under fully reversed cyclic plane bending moment ( $R = -1$ ), or pulsating bending moment ( $R = 0$ ).

To conduct a quantitative analysis of the development of fatigue slip-bands, the scanning atomic force microscopy (AFM) was employed for the present study. The scanning area for the observations was 30  $\mu\text{m}$  30  $\mu\text{m}$ . Since it was very difficult to identify in advance where fatigue cracks would be initiated, replicas of the specimen surface were taken at the predetermined number of fatigue cycles. The replica films were coated by gold (Au) before observation. The replications were conducted at the maximum tensile stress. Although the height of the surface in the replica film was reversed from the specimen surface, the height of the replica film in the AFM images was reversed by an image processing technique.

## EXPERIMENTAL RESULTS

### *Transgranular Cracking*

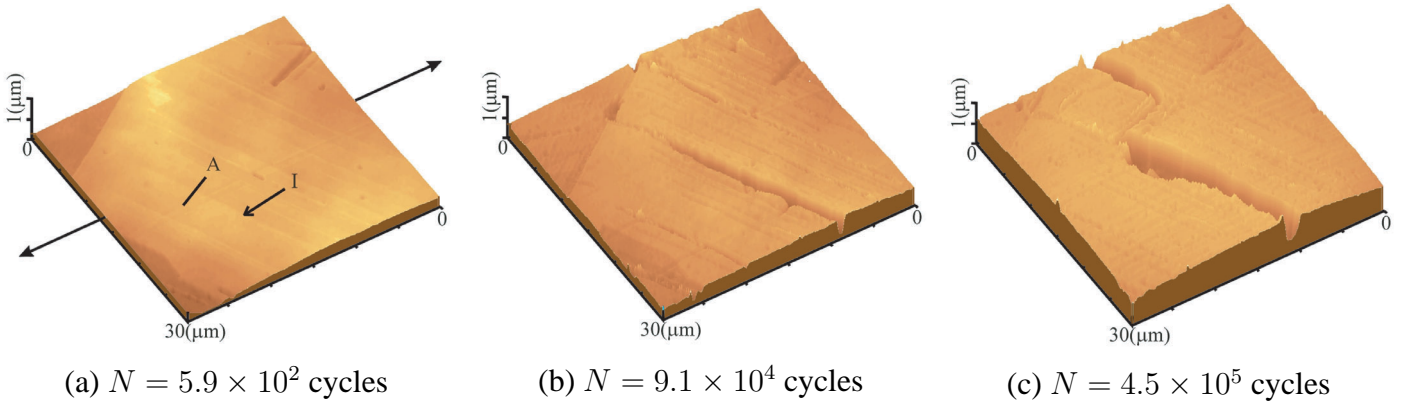


**Figure 1:** AFM images of transgranular cracking ( $\sigma_a = 173$  MPa, Material A).

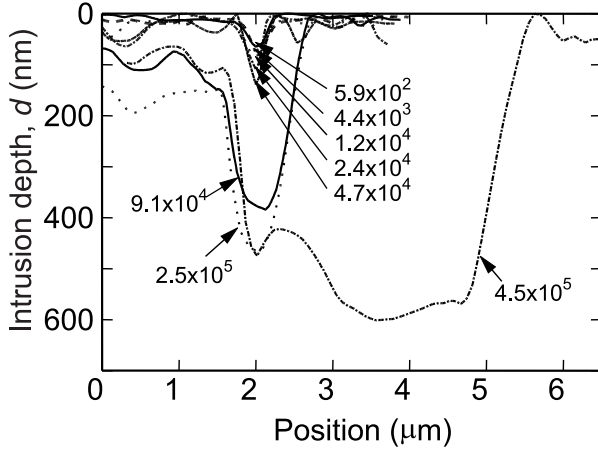


**Figure 2:** Change of intrusion geometry in fatigue ( $\sigma_a = 173$  MPa, Material A).

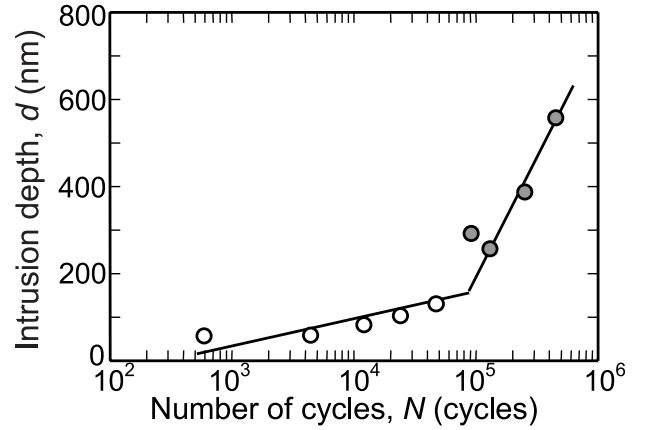


**Figure 3:** Change of intrusion depth in fatigue ( $\sigma_a = 173$  MPa, Material A).

In this section, the conditions for the crack-initiation in  $\alpha$ -brass will be discussed as a function of slip-band angle relative to the stress axis, stress amplitude, mean stress, and grain size. In  $\alpha$ -brass, fatigue cracks were initiated either from slip bands or along grain boundaries.

Another example of transgranular cracking process is shown in Fig. 1. It is clear from these AFM images that two parallel fatigue cracks were initiated at  $N = 9.1 \times 10^4$  cycles (Fig. 1 (b)), and they were coalesced at  $N = 4.5 \times 10^5$  cycles (Fig. 1 (c)). The change of the geometry of Intrusion I at cross section A, which is indicated in Fig. 1 (a), is shown in Fig. 2. With crack-initiation at  $N = 9.1 \times 10^4$  cycles, the depth of the intrusion increased rapidly, and with coalescence of cracks at  $N = 4.5 \times 10^5$  cycles, the width of the cracks (intrusion) increased rapidly. Change of the depth of Intrusion I is shown in Fig. 3 as a function of the number of the fatigue cycles,  $N$ . Even though the measured value was not actual depth after crack initiation, the depth of the intrusion drastically increased with its outgrowth to a crack at  $N = 9.1 \times 10^4$  cycles.

From surface observation, cracks much shorter than the grain-size were not found. Even just after the initiation, a crack prevailed whole grain, and Stage I crack growth was not observed. In the thickness direction, however, the depth of intrusion changed continuously before and after the crack initiation, *i.e.*, no jumping in the depth of intrusion was observed. It may indicate that Stage I crack growth, which is a fatigue crack growth along a slip-band, occurred in the thickness direction.

### **Intergranular Cracking**

An example of the intergranular cracking is shown in Fig. 4. Slip-bands were formed in a grain on the right side of a grain-boundary, and they were parallel to the grain-boundary. Both intrusions and extrusions were observed in the grain. In the grain on the left side of the grain boundary, slip-bands are not observed. A fatigue crack was initiated from the grain-boundary at  $N = 4.6 \times 10^4$ . An intergranular crack was considered to have been initiated along grain-boundaries between grains with high Schmidt factor slip system and with low

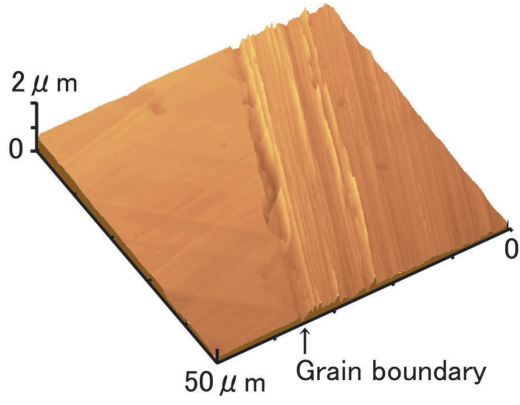


**Figure 4:** Intergranular fatigue crack initiation ( $\sigma_a = 110$  MPa,  $N = 7.9 \times 10^4$ , Material B).

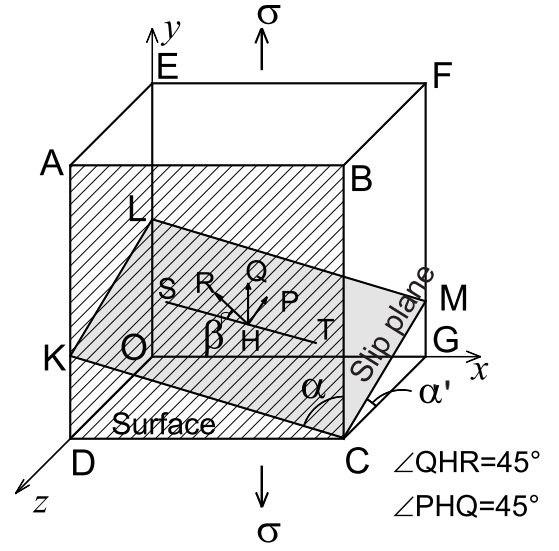


**Figure 5:** Slip-plane and directions relative to stress-axis and surface.

Schmidt factor slip system. The depth of the grain boundary,  $d$ , also increased with the number of cycles,  $N$ , and the crack-initiation could be easily identified from the change of the slope of the  $\log N - d$  relationship.

## DISCUSSION

Condition for the transgranular crack initiation is analyzed through a geometrical model proposed by Tanaka and Nakai [7, 8] shown in Fig. 5, which explains the relation between the surface-step and the slip-direction, where the Cube ABCDEFGO indicates a small region of a specimen that is located adjacent to the surface, and Point H is an arbitrary point on the slip-plane. In the figure, Plane ABCD represents the specimen surface, Plane CKLM represents the slip-plane, and  $y$ -axis and Arrow QH represents the loading-direction. Line CK is the slip-trace at the specimen surface and Line ST is a line on the slip-plane and that is parallel to Line KC. Arrow HR is the slip-direction on the slip-plane, and Arrow HP is the normal of the slip-plane. The surface-step induced by the slip is

$$d = s \cdot \sin \beta \cdot \cos \alpha', \quad (1)$$

where the value of  $s$  is the slip distance in the HR direction, the value of  $\alpha'$  is the angle between the normal to the surface and the trace of the slip-band on the plane that is perpendicular to the surface and parallel to the loading-axis, and the value of  $\beta$  is the angle between the slip-direction and the slip-traces on the surface (see Fig. 5).

Cracks are considered to have been initiated from slip bands, which had slip system in the maximum resolved shear stress [7, 8]. These slip bands are what is called as "persistent slip band (PSB)". For  $\angle QHR = \angle PHQ = 45^\circ$ , the resolved shear stress along the slip-direction takes the maximum value, and the following relationship should be satisfied.

$$\cos \beta = \sqrt{2} \cos \alpha. \quad (2)$$

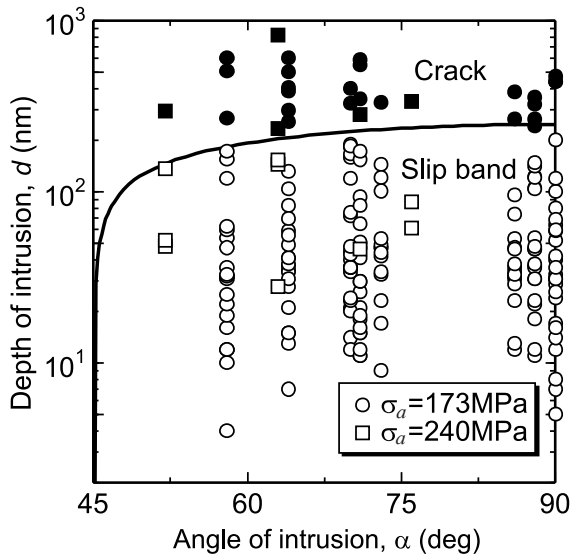
For  $\alpha = 90^\circ$ , the value of  $\beta$  should be  $90^\circ$ , which gives the maximum slip-step on the surface for a given slip distance. For  $\alpha = 45^\circ$ , the value of  $\beta$  should be  $0^\circ$  and no slip-step is formed on the specimen surface.

On slip-planes where the resolved shear stress takes the maximum value, the following equation should be satisfied.

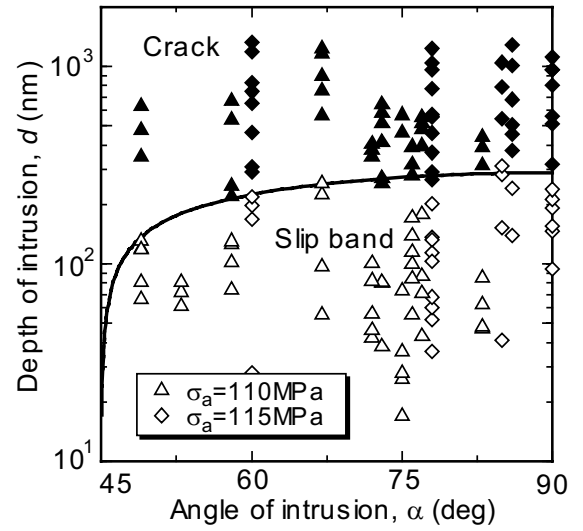
$$\cot^2 \alpha + \tan^2 \alpha' = 1. \quad (3)$$

The relation between  $d$  and  $s$  can be derived as a function of  $\alpha$  by substituting Eqs. (2) and (3) into Eq. (1).

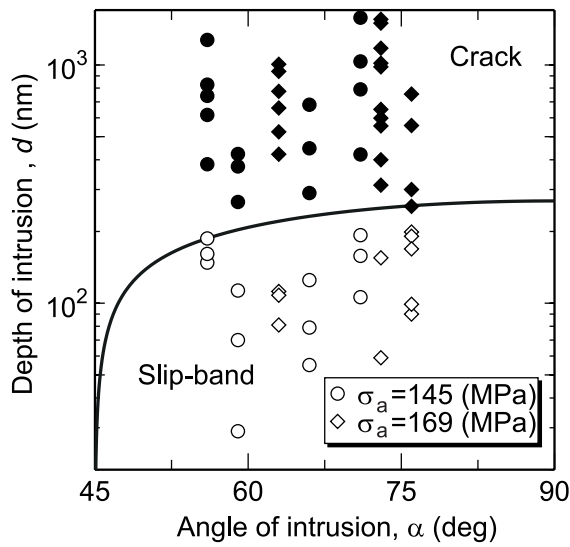
Figure 6 shows the depth of intrusions for various numbers of cycles as a function of the intrusion angle relative to the stress-axis. In the figure, data from the same intrusion fall on the same angle. Open marks indicate data



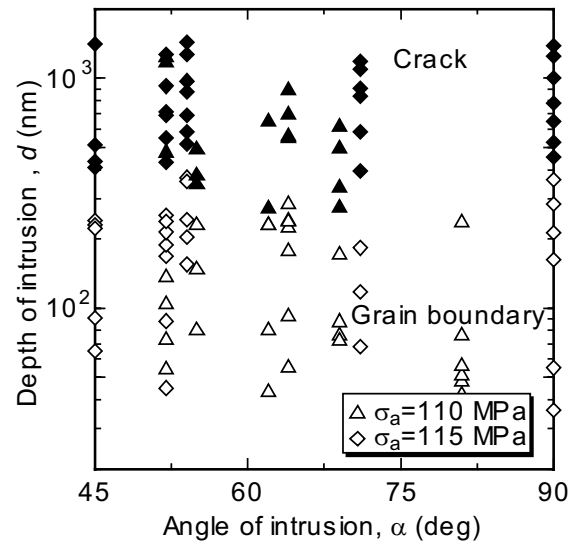
(a) Transgranular, Material A,  $R = -1$



(b) Transgranular, Material B,  $R = -1$



(c) Transgranular, Material A,  $R = 0$



(d) Intergranular, Material B,  $R = -1$

**Figure 6:** Fatigue crack initiation condition.

before the crack initiation, and solid marks show data after the crack initiation. The solid-lines in Fig. 6 show the relationship given from Eq. (1) for the value of  $s = 380$  nm. For the transgranular crackings, which are shown in Fig. 6, data before the crack initiation fall below the solid lines, and data after the crack initiation locate above the solid lines. It indicates that there was a critical value of accumulated slip-distance,  $s$ . The critical value of  $s$  was 380 nm, independent of the stress amplitude, the mean stress, and the grain-size. When the accumulated slip distance of an intrusion in a slip-band grew up to the critical value, a cracks was initiated from the intrusion. These results indicate that the transgranular crack initiation is controlled by the damage accumulation due to the dislocation substructures rather than the stress concentration induced by the intrusion.

As shown in Fig. 6 (d), the grain boundary depth at the intergranular crack initiation was not a unique function of the grain boundary angle relative to the stress axis. Other mechanism for the intergranular crack initiation should be considered, which may include the incompatibilities of deformation between two adjacent grains.

Since the critical value of slip distance at crack initiation was independent of mechanical and metallurgical conditions, the effects of these parameters on the fatigue crack initiation life should be attributed to their effect on the growth rate of slip distance. Therefore, the effects of the intrusion angle and the slip line length on the growth rate of the intrusion depth were examined. As shown in Figs 7 and 8, the rate was controlled not only by the intrusion angle and the slip-line length. It was affected by many factors, for example, constraint of deformation from adjacent grains. However, it is easy to predict when the depth reaches the critical value

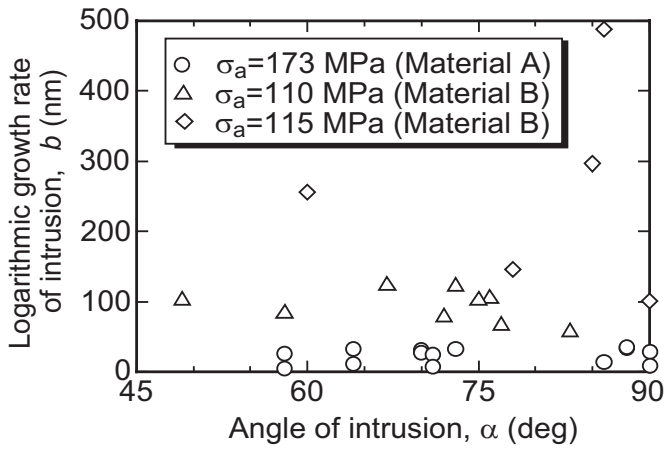


**Figure 7:** Growth rate of intrusion as a function of intrusion angle.

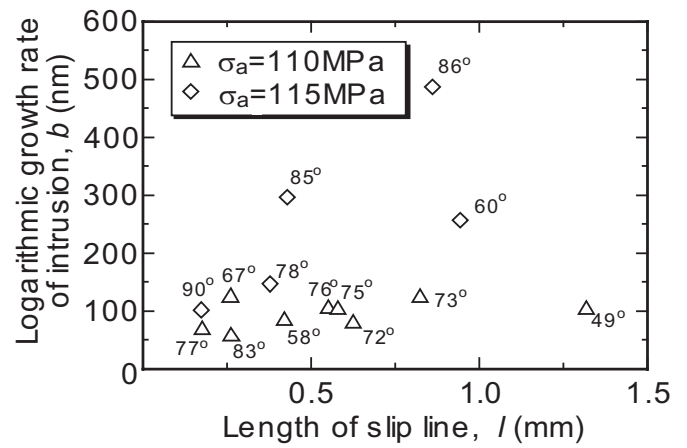


**Figure 8:** Growth rate of intrusion as a function of slip-band length.

because the intrusion depth increased linearly with the logarithm of the number of cycles like Fig. 3. Therefore, the location and remaining life of fatigue crack initiation can be predicted by measuring the intrusion depth few times before the crack initiation.

## CONCLUSIONS

The fatigue slip-band formation and the fatigue crack-initiation process in 70-30 brass were observed by means of AFM, and the following results were obtained.

- (1) The depth of an intrusion drastically increased with its outgrowth to a crack, and with coalescence of cracks, the width of cracks increased rapidly.
- (2) For the transgranular crack initiation, the intrusion depth at the crack initiation depended on the slip-band angle relative to the stress axis. At crack initiation, the slip distance in the slip direction, however, was constant independent of the slip-band angle, the stress amplitude, the mean stress, and the grain size.
- (3) Intergranular cracks were formed along grain-boundaries between highly deformed grains and grains without activating slip systems. For the intergranular crack initiation, the value of the intrusion depth (the grain boundary depth) at the crack initiation was not a unique function of the grain boundary angle relative to the stress axis.

## REFERENCES

1. Tanaka, K. (1987). *JSME Int. J.*, 30, 1.
2. Nakai, Y., Hiwa, C., Imanishi, T., and Hashimoto, A. (1999). *Proc. Asian-Pacific Conf. on Fracture and Strength '99*, SM22 (CD-ROM).
3. Nakai, Y., Fukuhara, S., and Ohnishi, K. (1997). *Int. J. Fatigue*, S223.
4. Nakai, Y., Ohnishi, K., and Kusukawa, T. (1999). *Trans. Jpn Soc. Mech. Eng.*, 65A, 483.
5. Nakai, Y., Ohnishi, K., and Kusukawa, T. (1999). In: *Small Fatigue Cracks: Mechanics and Mechanisms*, pp. 343-352, Ravichandran, K. S., Ritchie, R. O., and Murakami, Y. (Eds). Elsevier, Oxford.
6. Nakai, Y., and Kusukawa, T. (2001). *Trans. Jpn Soc. Mech. Eng.*, 67A, 476.
7. Tanaka, K., Nakai, Y., and Maekawa, O. (1982). *J. Mat. Sci., Jpn*, 31, 376.
8. Tanaka, K., Hojo, M., and Nakai, Y. (1983). In: *Fatigue Mechanisms: Advances in Quantitative Measurement of Physical Damage*, pp.207-232, Lankford, J., Davidson, D. L., Morris, W. L., and Wei, R. P. (Eds). ASTM STP 811.